RSC Advances

PAPER

View Article Online
View Journal | View Issue

Cite this: *RSC Adv.*, 2023, **13**, 28951

Enhancing the Ag-loading capacity on $Ti_3C_2T_x$ sheets as hybrid fillers to form composite coatings with excellent antibacterial properties†

Yajun Deng, * Zijie Zhou, Changan Zhang, Hui Li, Jianfeng Lan, Jianhua Wu and Shibin Wang

The settlement of microorganisms is an unwanted process in various practical fields, where also the first attaching microorganisms could promote other bacterial adhesion, causing an acceleration of bioaccumulation on the solid surface and damage to the surface functions. Developing an advanced composite coating with anti-microorganism attachment features is still a big challenge, and the critical element in any such method is to find an efficient functional agent for use in the coating system that could extend the service period. MXenes have received increasing attentions owing to their unique layer structure and large specific surface area. Increasing studies have been devoted to the development of MXene/polymer composites with creatively designed structures to realize various specific functions. Herein, two-dimensional (2D) transition metal carbide material MXene as a carrier was etched and decorated with cellulose to enhance the anchor points to grasp functional Ag nanoparticles *via* a simple method. The MXene nanosheets ($Ti_3C_2T_x$) were modified by cellulose to graft hydroxy groups on their surface, and then they were incorporated into silver nanoparticles (Ag NPs). The results showed that the cellulose could increase the loading content of the Ag NPs on the MXene surface, and also could act as a stabilized material to form the composite filler MXene@cellulose@Ag NPs (MAC), which could serve as a functional agent. Furthermore, the obtained product MAC filler exhibited excellent dispersibility and stability among all the tested fillers (MXene and MA), and it could help avoid aggregation and promote homogenous dispersal in the coating network. Besides, MAC displayed outstanding antibacterial activities against *E. coli* and *S. aureus* at the same concentration among all the fillers. When the filler was embedded into the coating system, the composite coating PCB-MAC possessed abundant active Ag^+ ions released by the Ag NPs, which could work against bacterial growth and achieve a favorable antibacterial inhibition effect. Therefore, we believe that the active MAC filler maintained high antibacterial efficiency, evincing its potential as a desirable agent for obtaining an excellent anti-adhesive behavior in numerous broad applications, such as the environment field or medical area.

Received 1st August 2023
Accepted 15th September 2023

DOI: 10.1039/d3ra05188a

rsc.li/rsc-advances

1. Introduction

Microorganism attachment is a common phenomenon in various application fields, including medicine, food, and even ocean engineering, resulting in potential safety hazards. Microorganism attachment is the preliminary behavior toward supporting a nutrient microenvironment that can facilitate other organisms to adhere, and bacteria growth is then ubiquitous and could easily generate a biofilm when attaching on a target surface. To confront this challenge, much effort has been devoted to exploring surface treatment or surface modification methods to achieve an improved bacterial resistance performance. One of the surface treatment methods is to cover the antibacterial film or coat the antibacterial organic material hybrids; for example, selecting the appropriate active additives to incorporate with an organic coating to form a composite.

MXene, which is a class of 2D transition metal carbide, has attracted considerable attentions since its discovery in 2011 by Gogotsi.[1–4] MXenes are classically obtained *via* etching selectively an A layer from an $M_{n+1}AX_n$ precursor, where M represents the transition metal elements, A represents the group 3 and 4 elements, X denotes N or C, and n is generally 1 to 3. Therefore, the $M_{n+1}AX_n$ structure is formed of $M_{n+1}X_n$ layers and obtains the 2D dimensional structure $M_{n+1}X_nT_x$, where T_x represents the terminal groups, such as –OH, –O, –F.[5–7] Owing to their excellent properties, such as metallic conductivity, and mechanical and

Xiamen Key Laboratory of Marine Corrosion and Intelligent Protection Materials, Jimei University, Xiamen, 361021, China. E-mail: dengyj@jmu.edu.cn

† Electronic supplementary information (ESI) available: The Ag NPs loading amount of MA and MAC fillers were added into "ESI". See DOI: https://doi.org/10.1039/d3ra05188a

thermal stability, these materials are applied to reinforce a polymer matrix to enhance its hardness, strength, and the other functional properties in many intensive potential applications in a variety of areas, such as membrane, coating, photocatalysts.[8,9] In particular, MXene is naturally hydrophilic and exhibits expedient decoration due to the terminal functional groups (–OH, –O, –F) on the surface, and the multilayer or few-layer structures are supporting a large specific surface area, suggesting it could be a promising carrier for advanced materials, and, particularly, a good candidate for preparing functional materials to potentially utilize in coating systems. However, MXene is unstable in humid environments and this disadvantage has obviously hindered its fabrication, storage, and even applications to date.[10] With regard to this problem, various methods have been proposed and adopted, such as storage in an inert environment, adding a functional agent, like antioxidant, anticorrosion, or antifouling additives, and decorating the surface by certain molecules or ions to achieve a stable microstructure.[11]

With inherent broad-spectrum antibacterial properties, metal ions are the most common and traditionally active bactericidal agents.[12,13] The conventional method to endow a coating with antibacterial performance is to introduce a suitable functional agent into the matrix, which could then develop the strong antibacterial properties. Silver nanoparticles (Ag NPs) are a kind of remarkable antibacterial agent. Therefore, adding Ag NPs onto the surface or into the interlayer of MXene could improve the antibacterial behavior and lengthen the durable antibacterial effect. Besides, the high specific surface area of MXene makes it a suitable template for immobilizing Ag NPs, which could address many problems of Ag NPs, such as their aggregation and cumulative toxicity, and could avoid the degradation of their active performances.[14–16] With regard to the outstanding antibacterial behavior of Ag NPs, according to studies, the specific process of killing the bacteria is as following. First, Ag^+ ions from the Ag NPs interfere with the bacterial cell membrane, attack the membrane, and disturb the transmembrane transport, leading to leakage of the cell content, deactivation of the functional proteins, and shrinkage of the genetic materials. Besides, Ag NPs can stimulate the formation of reactive oxygen species (ROS), which can affect the respiration enzymes to disturb the synthesis of ATP, lose the protein replication abilities, and eventually cause bacterial death.[17–21]

In a sense, the capacity to interfere in bacterial metabolism is closely related to the release of Ag^+ ions, and so herein, the loading amounts of Ag NPs was considered as an important key to promoting the enhanced antibacterial effect of MXene composites. Recently, Ag–Ti_3C_2 nanohybrids were fabricated *via* an *in situ* reduction method and exhibited excellent photodegradation efficiency due to the good conductivity of Ti_3C_2 and Schottky barriers of the interfacial Ag–TiO_{2-x}.[22] This method revealed that the assistance of MXene could stabilize the Ag NPs in the hybrid system, and boost their efficient function in photocatalysis. Zhou *et al.* explored the antibacterial property of hierarchical MXene@Ag hybrids prepared in an *in situ* reduction way, and the results showed that the bacterial killing behavior of the composite epoxy resin could be improved effectively.[23] Unfortunately, the *in situ* reduction of Ag NPs on the MXene surface led to some obvious disadvantages, including a durability deficiency, heterogeneous morphology, and a small amount loading on the MXene surface.

Herein, in this work, two-dimensional transition metal carbide material MXene with a large specific surface area was utilized as a carrier after decorating with cellulose. The cellulose was added to enhance the stability of MXene and to increase the anchor points to grasp the reinforced agents, *i.e.*, the Ag NPs. This method aimed to increase the loading contents of Ag NPs and to enhance the stability of the MXene@cellulose@Ag NPs (MAC) hybrid agent. Furthermore, on the basis of a previous work, polybenzoxazine resin PCB[24] was chosen as the carrier for the different fillers to evaluate the antibacterial properties in the composite coating network. It is believed that the prepared active agent and the composite coating have great potential for applications in medical equipment or for antibacterial surfaces.

2. Experimental section

2.1 Materials

Ti_3AlC_2 powder and silver nitrate ($AgNO_3$) were provided by Macklin Co., Ltd. Polyethyleneimine (PEI, M_w = 10 000 g mol^{-1}), lithium fluoride (LiF), hydrochloric acid (HCl), acetone, and ethyl alcohol were purchased from Sinopharm Chemical Reagent Co., Ltd. Ethylene glycol (EG), polyvinylpyrrolidone (PVP), and cellulose were obtained from Sigma-Aldrich. All the commercial chemicals were used as received.

2.2 Preparation of the $Ti_3C_2T_x$ and functional $Ti_3C_2T_x$ sheets

$Ti_3C_2T_x$ sheets were modified according to a previous method through the following steps:[25] (1) 1 g Ti_3AlC_2 powders as the precursor were added into an etchant solution containing 12 M LiF and 9 M HCl, and then the mixture was continuously stirred at room temperature for 24 h; (2) the obtained mixture was washed with deionized water and transferred to a centrifuge (3500 rpm) to remove the residual acid until the solvent pH value reached 6–7; (3) the $Ti_3C_2T_x$ sheets were ultrasonically dispersed in deionized water and further centrifuged to obtain a solid, and finally $Ti_3C_2T_x$ powders were obtained after 48 h freeze-drying.

Next, 100 mg of the as-obtained $Ti_3C_2T_x$ powders and 400 mg PEI were ultrasonically dispersed in 200 mL deionized water, and vigorously stirred for 24 h at room temperature. The mixture was washed with deionized water by centrifugation (3500 rpm) to obtain a solid. Finally, the modified powders (M-PEI) were collected after 48 h vacuum freeze-drying at −80 °C.

2.3 Fabrication of the MA and MAC fillers

The silver nanoparticles were fabricated by the following reported steps:[26] (1) silver nitrate ($AgNO_3$, 1.0 g), polyvinylpyrrolidone (PVP, 5.0 g), and ethylene glycol (EG, 500 mL) were added into a three-necked flask, and the mixture was continuously stirred at 130 °C for 2 h; (2) after 2 h stirring, the mixture was heated at 130 °C for 8 h without any stirring. Acetone was then added into the obtained mixture, and stirred

with ultrasonication for 5 min. Afterwards, the mixture was separated by centrifugation, washed by ethanol three times, and dried at 60 °C for 24 h to obtain the Ag NPs.

M-PEI powders (0.4 g), Ag NPs (0.6 g), and ethanol (200 mL) were added into 250 mL flask. The mixture was stirred at 30 °C for 60 min, and then the mixture was separated by centrifugation at 8000 rpm for 10 min, washed by ethanol twice, and collected by vacuum freeze-drying after 48 h at −80 °C. The powder was MXene@Ag nanocomposites (MA). The Ag NPs loading amount of the MA filler was about 24.1 wt% of the total mass fraction, as shown in Fig. S1 and S2.†

Cellulose (0.8 g) was mixed into ethanol (100 mL) and stirred for 3 min to obtain a homogenously dispersed solution. Then, 0.4 g M-PEI powders was added into the above solution and stirred for 30 min. After that, 0.6 g Ag NPs was added into the aforementioned mixture and then continuously stirred for 24 h. Finally, the mixture was centrifugated at 8000 rpm for 10 min, washed by ethanol twice, and vacuum freeze-dried for 48 h. The powder was MXene@cellulose@Ag nanocomposites (MAC). The Ag NPs loading amount of MAC filler was about 47.6 wt% of the total mass fraction, as shown in Fig. S3 and S4.†

2.4 Preparation of the composite polybenzoxazine resins

The composite polybenzoxazine resin was generally fabricated as follows: (1) benzoxazine monomer was prepared according to a previous work.[24] Specifically, curcumin (0.01 mol, 3.68 g), paraformaldehyde (0.04 mol, 1.20 g), and 3-aminopropyltriethoxysilane (APTES, 0.02 mol, 4.42 g) were added into a 250 mL flask filled with chloroform (100 mL) followed by stirring and refluxing for about 48 h at 96 °C. After the reaction had finished, the mixture was allowed to cool down and the product was separated and purified to obtain the pure benzoxazine monomer (CB). Then, the monomer was dissolved in tetrahydrofuran to form a homogeneous solution; (2) the nanocomposites, including MXene, MA, and MAC, were respectively dispersed in tetrahydrofuran, and the mixtures were ultrasonicated for 10 min, respectively; (3) the nanocomposite dispersions were separately added into the monomer homogeneous solution, and the mixtures were magnetically stirred for 8 h at 45 °C separately; (4) the redundant solvent was removed from the mixture *via* a rotary evaporator, and the concentrated mixture containing 5 wt% various nanocomposites was spin-coated onto cleaned glass plates (25 mm × 25 mm × 1.5 mm), which were respectively washed by acetone and ethanol; (5) all the coated samples were cured at temperatures from 60 to 200 °C at a heating rate of 20 °C/20 min, and then the samples were heated at 200 °C for 1 h. The coating containing the MXene, MA, and MAC nanocomposite were named as PCB-M, PCB-MA, and PCB-MAC, respectively. The PCB coating was prepared following the same procedures except for the addition of any nanocomposite. All the coating thicknesses were about 25 ± 5 μm.

2.5 Characterization

The Fourier transform infrared (FT-IR) spectra of the samples were conducted on a Nicolet iS50 spectrometer in the range from 4000 to 500 cm^{-1}. Surface morphology analysis of the nanoparticles was performed by scanning electron microscopy (SEM, Hitachi FE-SEM 4800, Japan) observation under 10 kV. The Raman spectra of the different nanoparticles were recorded on a confocal Raman spectrometer (LabRAM HR Evolution, Horiba, Japan) utilizing an excitation wavelength of 532 nm, with LabSpec6 software used for to process the Raman spectra. Thermogravimetric analysis (TGA, Netzsch STA 449F3 Jupiter, Germany) was performed at a heating rate of 10 °C min^{-1} under a N_2 flow with a 50 mL min^{-1} flow rate in the temperature range of 25–800 °C. The micromorphology of the nanoparticles was observed by transmission electron microscopy (TEM, Talos F200s, USA) under an acceleration voltage of 15 kV. Also, X-ray diffraction (XRD, D8-A25, Bruker axs) was performed to investigate the crystalline structure of the samples.

2.5.1. Antibacterial assessment. The assay was performed according to a previous method.[27] Specifically, *Staphylococcus aureus* (*S. aureus*, ATCC 6358P) and *Escherichia coli* (*E. coli*, DH5α), as the representative Gram-positive and Gram-negative bacteria are typically employed as indicators to judge the antibacterial activity. Various concentrations of the different nanotubes (including MXene, MA, and MAC at 0, 4, 12, 20, and 24 mg mL^{-1}) were charged into *S. aureus* or *E. coli* bacterial suspensions (1 mL, 1×10^7 cfus mL^{-1}) in conical flasks. The mixtures containing the nanotubes and the bacterial suspension were respectively incubated at 120 rpm in a shaking incubator at 37 °C for 12 h. Afterwards, 100 μL aliquots of the bacterial suspensions were respectively extracted and added into the Luria–Bertani agar plate, and then the plates were placed in the incubator at 37 °C for 24 h. Images of the bacteria were recorded. Each of the experiments was repeated at least three times.

2.5.2. Bacterial anti-adhesion of the different coatings. The antifouling performance of the coatings was evaluated according to a method in a previous work.[28] Specifically, the various coatings (10 mm × 10 mm × 1.5 mm) were respectively added into the bacterial suspensions (*S. aureus* and *E. coli*, 1×10^7 cfus mL^{-1}) in a 24-well plate, and the hybrid suspensions were cultured for 6 h at 37 °C under 120 rpm shaking. Afterwards, the bacterial suspensions were respectively extracted and the coatings were rinsed in sterilized phosphate buffer saline (PBS) solution to remove the unattached bacteria, and then Syto-9 (2 mg mL^{-1}) was added into the plate to stain the samples at 23 °C for 15 min in the dark condition. Finally, the bacteria on the various sample surfaces were observed using an Olympus IX73 fluorescence microscope.

2.5.3. SEM observation. The morphologies of the bacteria (*S. aureus* or *E. coli*) on the coating surfaces were separately observed and detected by SEM after the bacterial adhesive resistance test.[24] Specifically, the bacteria attached on the coating surface were rinsed by sterilized PBS twice, fixed with 2.5 wt% glutaraldehyde solution for 4 h, and then dehydrated for 10 min twice sequentially with 30%, 50%, 75%, 90%, and 100% ethanol. Finally, the morphologies of the dried bacterial on the coating surface were observed and recorded by SEM.

3. Results and discussion

This study focused on increasing the Ag NPs loading content on the surface of MXene by a novel and simple method. Through the greater loading of Ag NPs, while avoiding the aggregation of the Ag NPs, the antibacterial behavior of MXene could be improved. This represents a meaningful and promising approach to endowing the coating material with specific functions and to meeting the demands of the colloid surface in specific applications.

3.1 Morphologies and compositions of the microstructures

The synthesized MXene samples were prepared through a "top-down" method by using HF wet-etching to remove one or more atomic layers from the Ti_3AlC_2 phase to form the designed $Ti_3C_2T_x$. Herein, when the Al layer is etched away, the Ti_3C_2 naturally forms –O, –F, –OH, where T represents the terminating surface groups in the $Ti_3C_2T_x$ structure,[29] as shown in Fig. 1a. Then, the Ag nanoparticles (Ag NPs) were modified on the definite surface layer thanks to the addition of PVP and PEG,[28] and this layer was identified by the hydroxyl groups, which were utilized as anchors to hold the terminating sites on the $Ti_3C_2T_x$ sheets. Then, Ag NPs were directly loaded on the $Ti_3C_2T_x$ sheets for comparison, and this samples was named as the MA hybrid. To vividly demonstrate the three-dimensional structure, a schematic illustration of MA is provided in Fig. 1a. Furthermore, for increasing the anchors to hold more Ag NPs on the $Ti_3C_2T_x$ layer, one of the promising methods is to decorate the $Ti_3C_2T_x$ surface to meet the needs for higher loading concentrations. Cellulose was used here as a natural material that possessed the required hydroxyl groups to graft on the $Ti_3C_2T_x$ surface (as MC in Fig. 1b) and to enhance the

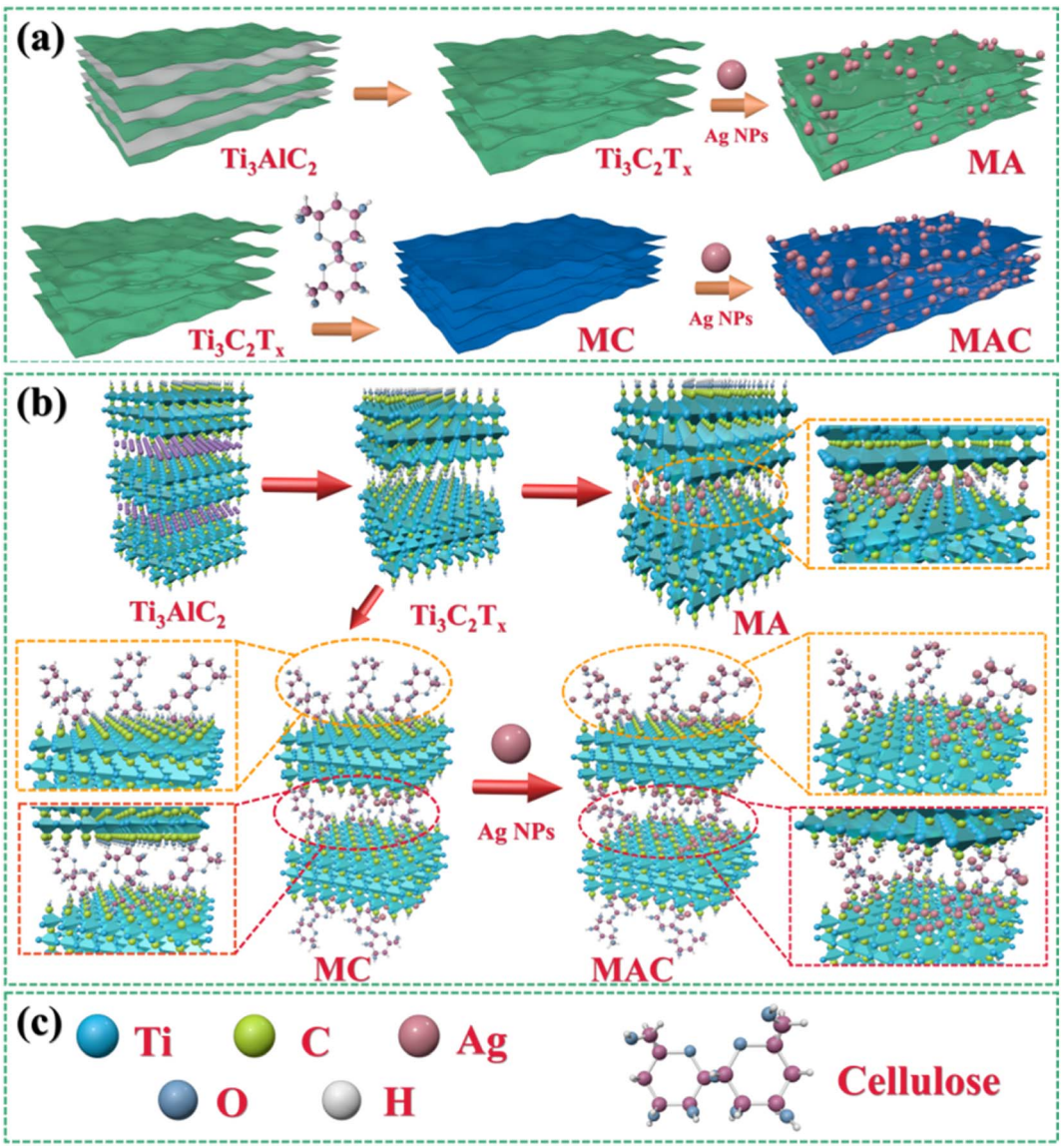

Fig. 1 . Synthesis methods and fabrication processes (a and b) for obtaining $Ti_3C_2T_x$ (MXene) by Ti_3AlC_2, MA, MC, and MAC;[30] (a–c) schematic illustration of the molecular model for $Ti_3C_2T_x$ (MXene), MA, MC and MAC.

holding sites to grasp more Ag NPs to form the target product MAC, as shown in Fig. 1a and b. Besides, the modification of MXene by cellulose could avoid the Ag NPs aggregation and enhance their dispersibility *via* the hydrogen or covalent bonds of the molecular links.

To prove the surface morphology and the structure composites of the different hybrids, SEM and TEM were used to accurately analyze the structural morphologies and composite elements of the MA and MAC hybrids, as shown in Fig. 2. As shown in Fig. 2A, the Al layer was removed from the Ti_3AlC_2 sheet to form the multilayer structure $Ti_3C_2T_x$ (MXene) after sufficient HF etching (Fig. 2a and b). The unique surface and interface engineering of MXene could provide a huge surface area containing functional groups such as –O, –OH, and –F, which could act as the sites to load the Ag NPs on the MXene layer *via* hydrogen bonding, van der Waals forces, and hydrogen bonding (Fig. 2c and d). However, the Ag NPs led to a lower loading *via* straightforward attachment on the MXene surface according to the images in Fig. 2c and d. The surface modification or functionalization of the carrier MXene has attracted much interest for directly quantifying nanomaterial species. Thus, by modifying the surface with cellulose as grafted-on chains, the MXene sheets can gain increased functional sites to anchor more Ag NPs, as shown in Fig. 2e and f. To confirm this, the following tests were done focused on the elements in the different fillers, including MXene, MA, and MAC. The TEM morphologies and element mappings of MA and MAC are presented in Fig. 2B and C, where it can be seen that MA and MAC showed dense Ag NPs on the MXene surface with the presence of clear diffraction sites of the $(0\bar{1}10)$, $(1\bar{1}00)$, and $(10\bar{1}0)$ facets, indicating the existence of MXene.[31,32] Also, the element mapping images demonstrated the uniform distributions of Ti, O, F, N, C, Ag, and Cl. As above-mentioned, the MXene modified by cellulose displayed a greater loading concentration of Ag NPs, obtained *via* a simple approach to achieve the desirable structure for endowing it with antibacterial properties, and thus making it a potential candidate for larger-scale use in future biological surface applications.

3.2 Characterization and analysis

In order to clarify the structural characterization, the chemical compositions of MXene, and the hybrids MA and MAC were measured by FT-IR, Raman, and XRD analysis. As shown in Fig. 3a, from FT-IR spectra, intense and broad absorption band ranges at 3277–3440 cm^{-1} could be observed, belonging to the –OH group, which was assigned to the combination of –OH on the $Ti_3C_2T_x$ nanosheets and the Ag NPs surface. Other peaks that appeared at 674 and 557 cm^{-1} corresponded to Ti–O and C–Ti characteristic vibrations.[33] Furthermore, absorption peaks at 2893 and 1630 cm^{-1} were noted and assigned to the C–H and C–O bending vibrations.[23] It was noted that the C–H and C–O groups were decorated on the surfaces of the Ag NPs and provided specific sites to anchor on the MXene nanosheets.

Besides, as shown in Fig. 3b in the Raman spectra, absorption peaks were observed at 1353 and 1574 cm^{-1}, which were attributed to C–N and C=C groups of the different nanocomposites and caused by the remaining surfactants or the reducing agents from oleic acid, oleylamine, or ascorbic acid on the Ag NPs. The absorption peaks of MAC were stronger than those of the MA owing to the grafted cellulose on the MXene surface.[34] To further prove the successful preparation of MXene, and hybrids MA and MAC, the XRD patterns of the various samples were obtained and are shown in Fig. 3c. It could be seen that the characteristic peaks appeared at 28.0° and 61.0°, which corresponded to the (008) and (110) crystal faces of MXene.[23,35] The peaks at 38.2°, 44.4°, 64.54°, and 77.0° respectively belonged to the (111), (200), (220), and (311) crystal faces of Ag NPs, and were close to the reported values,[36,37] indicating

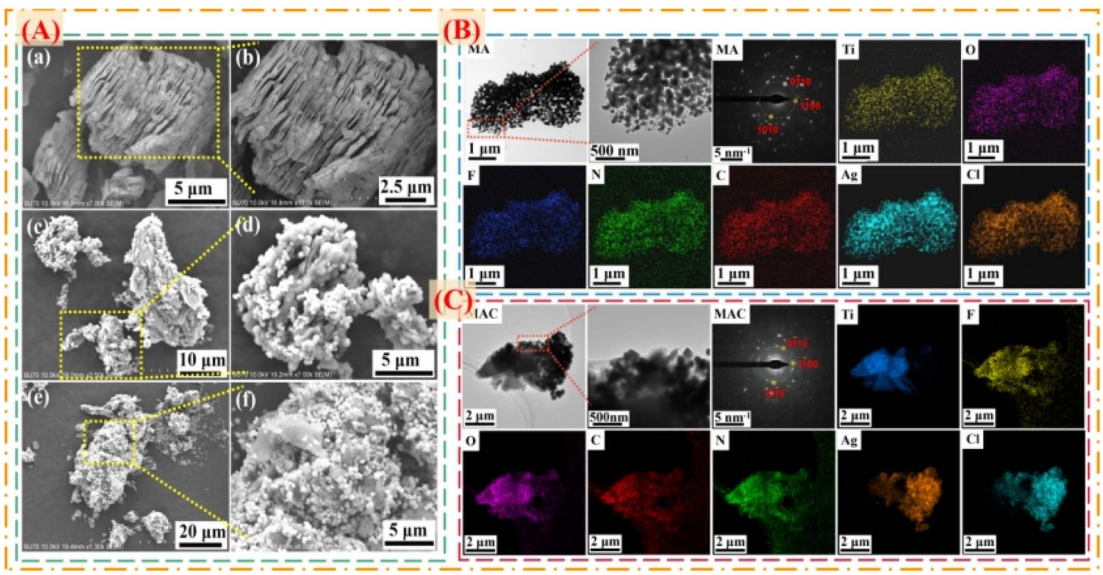

Fig. 2 (A) SEM images of the composite fillers of (a and b) MXene, (c and d) MA, and (e and f) MAC. TEM, SAED, and elemental mapping images of (B) MA and (C) MAC.

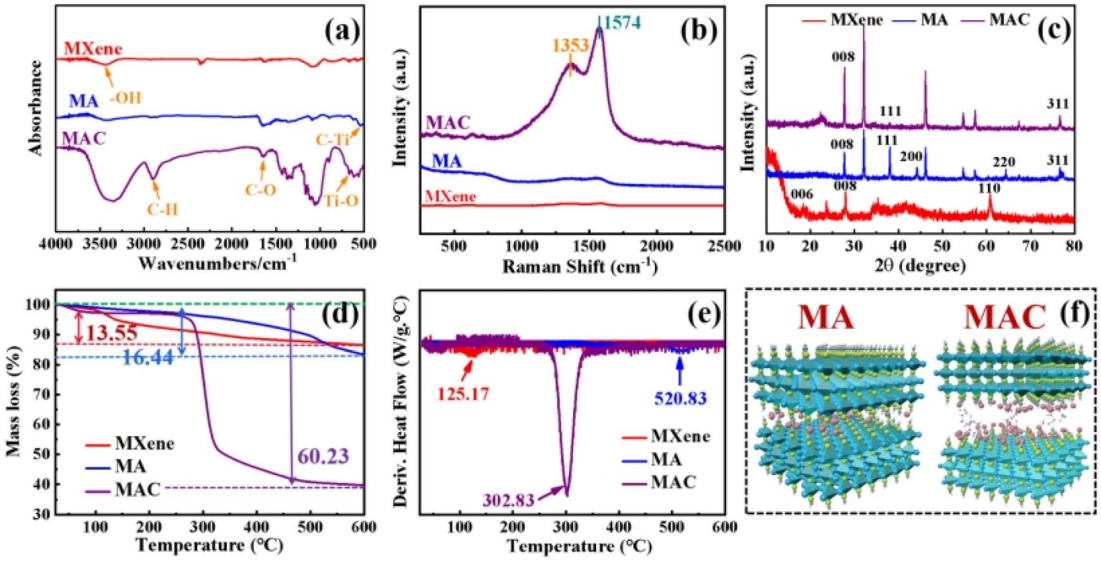

Fig. 3 (a) FT-IR spectra of the different composites (MXene, MA, and MAC); (b) Raman spectra of the different composites; (c) XRD patterns of the different composites; (d) TG and (e) DTA curves of the different composites; and (f) molecular models of MA and MAC.

the enrichment of the crystallinity of Ag NPs with the increasing concentrations of nanoparticles. Due to the higher loading concentrations of Ag NPs on the MXene surface, the specified peaks for MAC were stronger than those of the MA hybrid. This was due to the functional groups of cellulose on the MXene surface, which acted as the crucial sites to hold the dense Ag NPs, and these results were consistent with the morphologies obtained by the SEM and TEM analysis. All the aforementioned analyses demonstrated the successful preparation of the composites MA and MAC.

Thermogravimetric analysis was next performed and showed that the different fillers MXene, MA, and MAC exhibited decreased thermal stability. MXene was most thermally stable, with an 86.47% char yield, which was higher than that of the hybrids MA and MAC with 83.38% and 39.71% char yields, respectively. Because of the organic units of the Ag NPs surface on the MXene, MA showed less stability and its maximal weight loss was at 520.83 °C, as shown in Fig. 3d, e, and Table 1. Utilizing cellulose as the grafted-on chains to modify MXene, the MAC composite developed the lowest char yield of 39.71%, and showed the maximal weight loss at 302.83 °C, owing to the degradation of the grafted cellulose on the MXene surface and/or the organic units on the Ag NPs surface. From the above characterization results, the MA and MAC hybrids were further identified by their structure, and the desired molecular models could thus be described, as shown in Fig. 3f, to explain their morphologies and microstructures.

Table 1 Thermal parameters from the TG and TGA curves of the different fillers

Sample	$T_{5\%}$ (°C)	$T_{10\%}$ (°C)	$T_{max\%}$ (°C)	Char yield (%)
MXene	137.67	328.17	125.17	86.47
MA	352.83	492.33	520.83	83.38
MAC	275.00	288.17	302.83	39.71

3.3 Static settlement and stability of the different fillers

The dispersion stability of the different fillers, including MXene, MA, and MAC, was studied and is shown in Fig. 4. The zeta potentials of MXene, MA, and MAC with negative charges were respectively around -2.52 ± 0.98, -4.57 ± 0.23, and -7.27 ± 0.43 mV, as shown in Fig. 4a. The negative zeta potential value of MXene showed a higher negative charge owing to their aggregation in the ethanol dispersion. Due to the uniform structure of hydroxy groups on the Ag NPs surface, the MA dispersion showed a lower potential value than MXene, indicating the MA dispersion was more stable than that of MXene. Besides, the MAC dispersion displayed the lowest potential value. These results implied that cellulose served as a stabilizing agent for the MAC and could effectively avoid the Ag NPs aggregation and greatly enhance the dispersibility of the as-prepared solution. Actually, the optical photograph images in Fig. 4b of the different fillers could directly show the dispersion stability. As with the experimental results, the different fillers in ethanol solutions were homogeneous and uniform, with MXene exhibiting rapid sedimentation, causing the solid–liquid separation after 1 hour settlement. After 5 h settlement, MA showed a clear separation of the solid–liquid phase and a solid aggregation at the bottom of the bottle. MAC displayed the most stability compared to the MXene and MA fillers, and it exhibited agglomeration after 15 hours settlement. This phenomenon of the fillers was the same as shown in the zeta potential analysis. All the observations further confirmed that the target filler had been obtained, and the good stability of the MAC mixture could promote the compatibility between the coating and active filler to achieve the composite coating stabilization for the solid surface of medical devices.

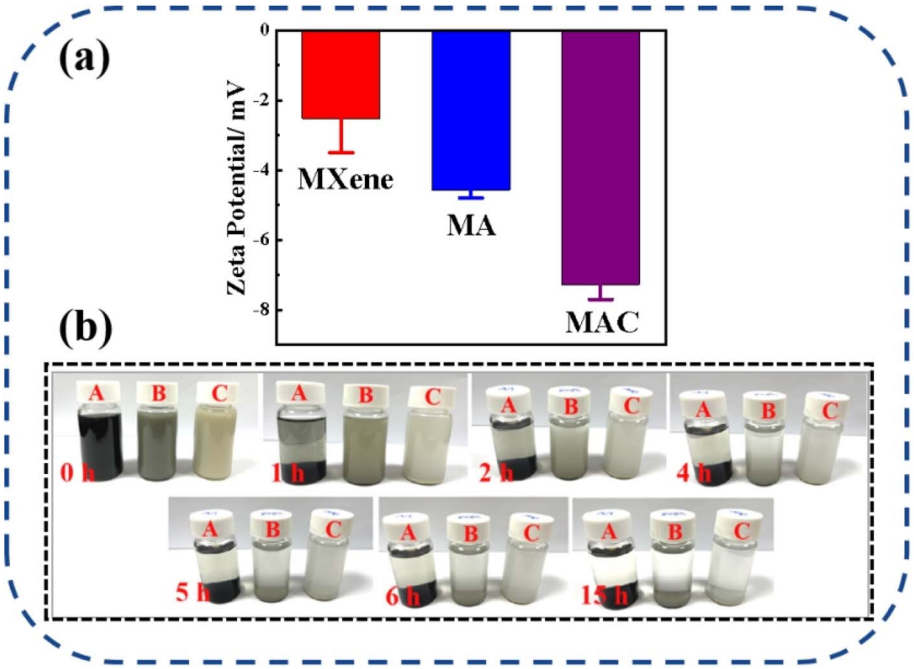

Fig. 4 (a) Zeta potentials of the different fillers (MXene, MA, and MAC) in ethanol dispersion, (b) images of the different fillers with their static settlement, where A = MXene, B = MA, and C = MAC.

3.4 Antibacterial and anti-adhesive performances

As noted, biofouling is a negative impact and serious challenge to the protective coating used in many applications. Nanotechnology and the use of a polymer composite are two efficient methods to satisfy the need for a colloid surface to improve the antibacterial properties. The use of an active antibacterial agent is a directly valid method to enhance the functionalization of a coating. Herein, bacteria *E. coli* and *S. aureus* were used as indicators to evaluate the bacterial killing behavior of the agents. To probe the exact concentration needed to inhibit the growth of these two kinds of bacteria, different concentrations of the active agents, such as 0, 4, 12, 20, and 24 mg mL^{-1}, were respectively added into the bacterial suspensions, and those suspension were extracted and added on to a Luria–Bertani agar plate to culture in the incubator. After 6 h incubation, the colonies of both *E. coli* and *S. aureus* were recorded to assess their growth situation. As shown in Fig. 5a and b, the comprehensive optimum concentration of the agent was 20 mg mL^{-1}, which was found could best disturb the bacterial growth and reproduction, while MXene showed low antibacterial activity even at the highest concentration (24 mg mL^{-1}). On the one hand, MXene exhibited some antibacterial capacity because it has sharp edges, which could destroy the adsorbed bacterial cell membrane *via* oxidation and physical processes.[38] Besides, the abundant surface groups on the MXene surface when connecting with the bacterial membrane could promote the loss of bacterial nutrients and deactivate the cytoplasm of the cells through hydrogen bonding.[39] On the other hand, relative to the Ag NPs, MXene showed an obviously weak antibacterial capacity. Thus, the synergistic effect of the Ag NPs to form a composite agent is an effective and important method for enhancing the antibacterial activity of MXene.

As for the aforementioned optimum antimicrobial concentration, we choose the agent concentration at 20 mg mL^{-1} to embed into the benzoxazine monomer to form the composite mixture and heat-cured it to give the crosslinked hybrid resins. Different resins containing the agents MXene, MA, and MAC were obtained and respectively named as PCB-M, PCB-MA, and PCB-MAC. The bacteria *E. coli* and *S. aureus* settlement on the different coatings surface was assessed, as shown in Fig. 6A, and the fluorescence intensity and efficiency of the stained coating surfaces were compared, as shown in Fig. 6B(a) and (b). Compared to the results for the fluorescence intensity of bare glass, the coatings including the PCB and the composite coatings (PCB-M, PCB-MA, and PCB-MAC) showed less bacterial attachment on the staining surface, and the fluorescence intensity of the PCB-MAC coating observed on the surface was the lowest brightness, compared to that of the control bare glass and other composite coatings. These results demonstrated that PCB-MAC exhibited a better antifouling activity against the bacteria, and the highest fluorescence efficiency.

To clearly explore the growth states of the bacteria and the killing results by the active agents, the completed condition of the bacteria on the coating surface were observed to visualize the damaged morphologies of the bacterial membrane *via* SEM measurement, and the results are shown in Fig. 7A and B. PCB was used and tested as the control coating. It was found that *E. coli* seeded on the PCB surface with an intact rod shape, while the bacteria on the PCB-M coating surface had obviously shrunk and even caused holes to appear. Seriously, for the bacteria on the PCB-MAC coating, their membrane became rougher and

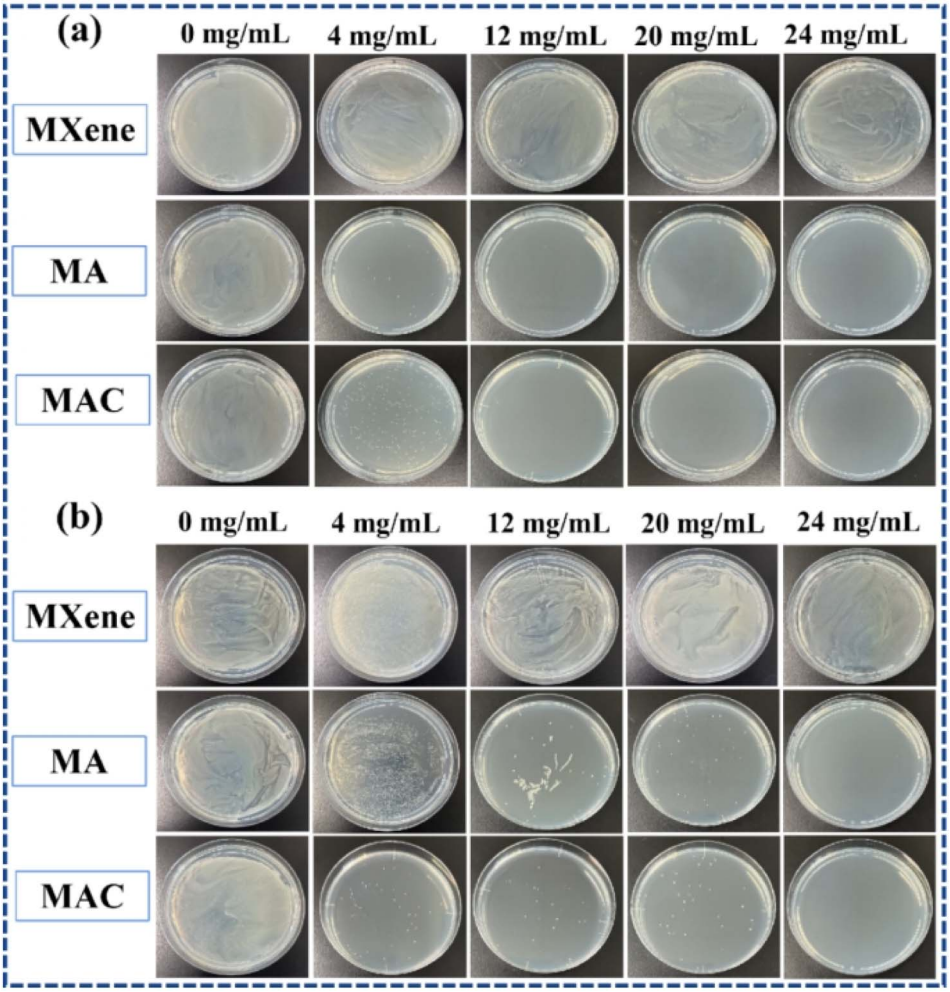

Fig. 5 Bacterial plate photos of (a) *E. coli* and (b) *S. aureus* incubated with different concentrations of the composite fillers of MXene, MA, and MAC for 6 h incubation with 0 (control), 4, 12, 20, and 24 mg mL^{-1} concentrations, respectively.

more damaged than those on the PCB-MA surface. It could be clearly observed that most portions of the bacteria on the PCB-MAC coating were even destroyed. Likewise, *S. aureus* on the PCB and PCB-M coating surfaces exhibited a spherical shape with integrated and smooth membranes, while those bacteria seeded on the PCB-MA and PCB-MAC were seriously shrunk and showed damaged cells, which permeated with obvious lysis from the cell. The PCB-MAC coating revealed the best antibacterial behavior caused by the slow release of Ag^+ ions, which could then attack the cell membrane and disturb the transmembrane transportation, thus damaging the bacterial metabolism.

A detailed schematic diagram of the bacterial killing activity of the PCB-MAC coating is shown in Fig. 8, where the significant antibacterial property of this coating was derived from the active filler MAC. Silver, one of the most well-known antibacterial agents, has been widely utilized to enhance the biocidal activity of materials, including the MXene sheet here. A prior interesting research reported that $Ag/Ti_3C_2T_x$ was a better synergistic antibacterial model combining MXene with Ag^+ release under special NIR irradiation, relative to Ag NPs or MXene alone.[40] The composite antibacterial action has two keys factors. On the one hand, MXene enabled a larger surface area and improved sharp edges of the two-dimensional sheets, which could promote a better antibacterial property. Besides, the negative surface charges on the MXene surface were less effective against *E. coli*, which is a Gram-negative bacteria and can form a higher resistance to MXene sheets.[41,42] On another hand, Ag NPs exhibited excellent antibacterial activity. The protons and the dissolved oxygen reduce the production of hydrogen oxides that would otherwise accelerate the oxidation of Ag to form unstable Ag^+ ions.[19,20,43–45] The Ag^+ species from the Ag NPs reservoir could penetrate the bacterial cell membranes containing an outer membrane and inner plasma membrane to disturb the transmembrane transport. Thus, the Ag^+ ions stimulate reactive oxygen species (ROS), which is a natural by-product of oxygenic respiration.[46] The cell then endures high oxidative stress, leading to a cellular inactivation,[47,48] including from the ROS attacking the protein to denaturalize physiological functions, and hinder the replication of DNA and mRNA, as well as damaging the bacterial metabolism. The outstanding sterilizing effect is thus related to the higher release

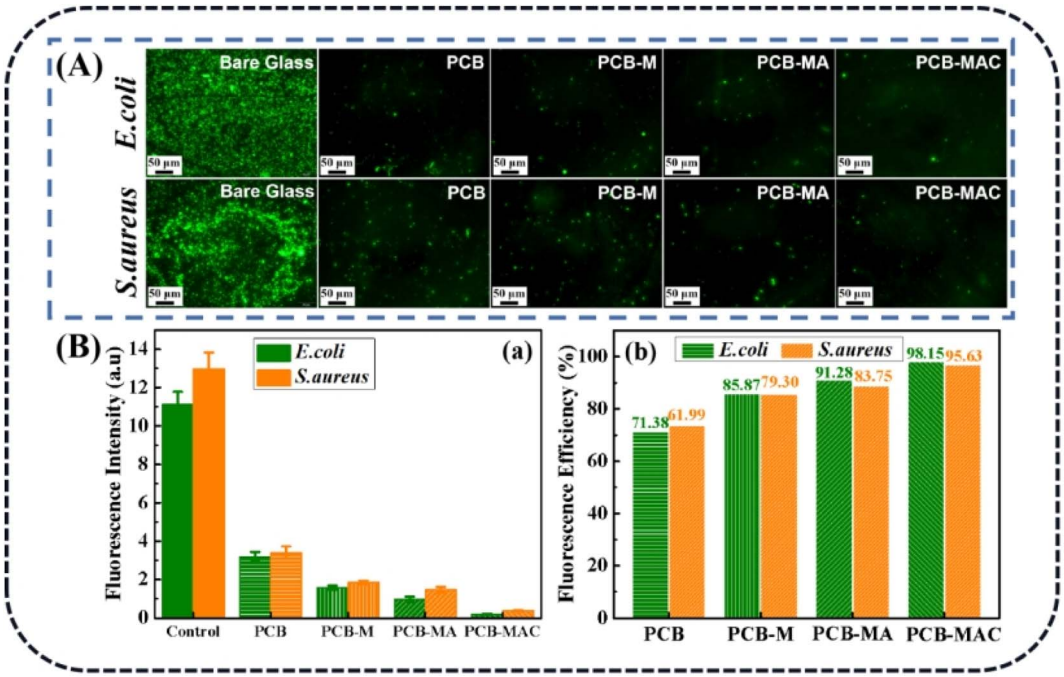

Fig. 6 (A) Fluorescence microscopic images of the bacteria *E. coli* and *S. aureus* settled on different surfaces after 6 h of immersion in bacterial suspensions, (B)(a) fluorescence intensities and (B)(b) fluorescence efficiencies relative to bare glass of *E. coli* and *S. aureus* settled on different surfaces.

concentration of Ag^+ ions. Herein, the MAC agent showed obvious advantages because it utilized the MXene as a carrier to load more Ag NPs to avoid the aggregation of nanoparticles, and it could thus display excellent antibacterial activity at the same agent concentration when compared with the other agents in this work.

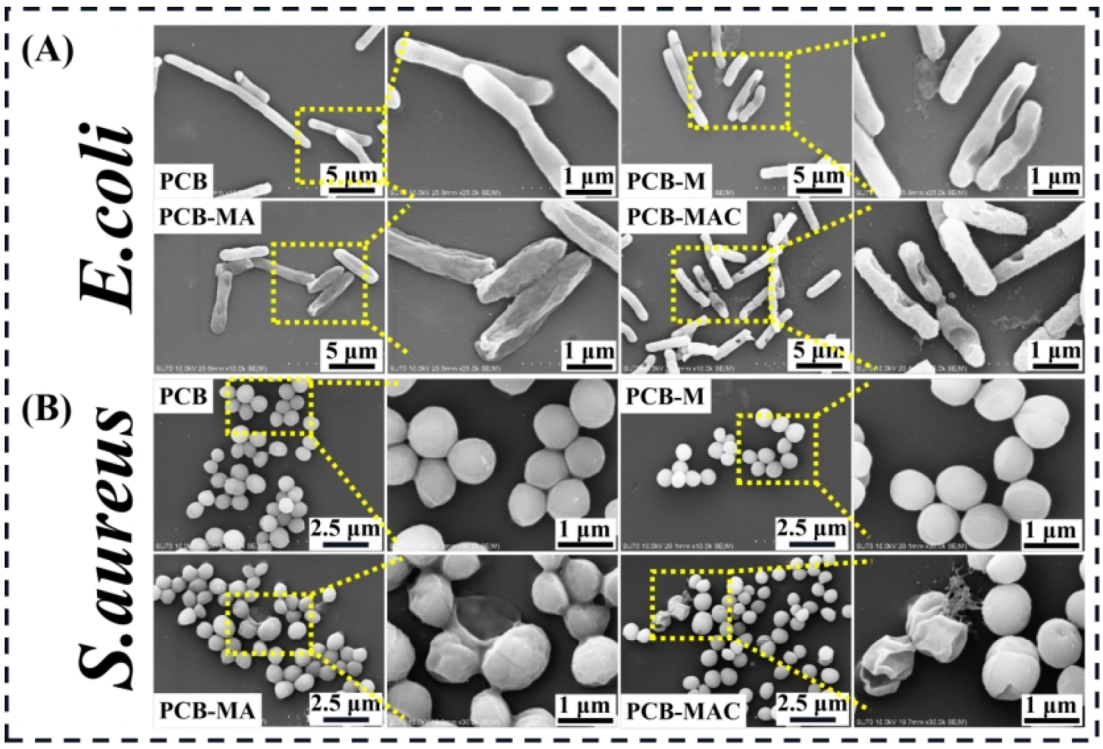

Fig. 7 SEM microscopic images of the bacteria (A) *E. coli* and (B) *S. aureus* attached on the surfaces of the coatings PCB, PCB-M, PCB-MA, and PCB-MAC.

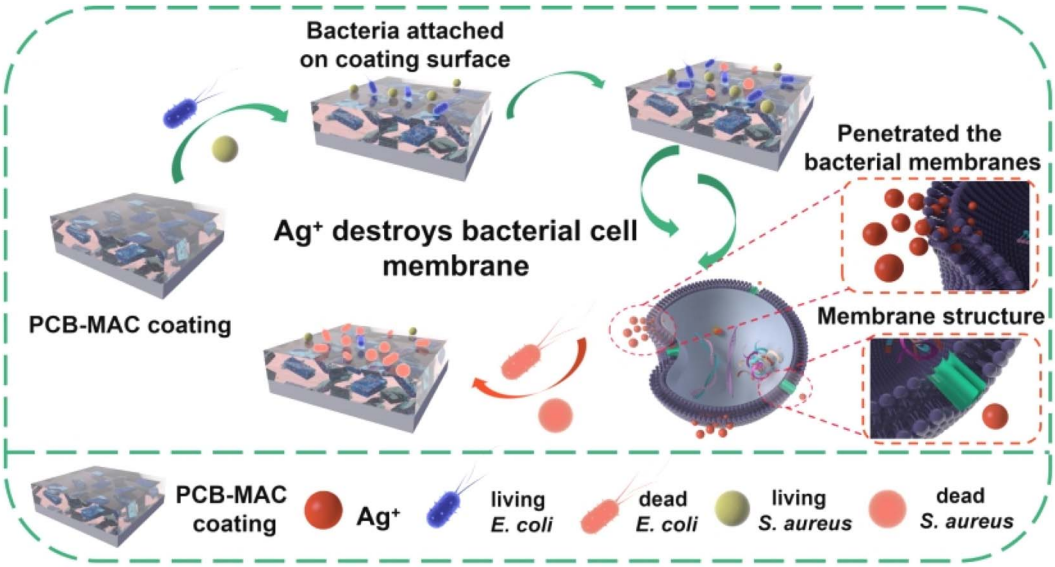

Fig. 8 Schematic diagram of the antibacterial mechanism of the Ag nanoparticles.

Based on the practical applications of MXene-based materials, these materials would need to take into consideration the possible toxicities. There are several comprehensive research reports on the evaluation of MXene composite agents. MXene can cause some cell cytotoxicity, attributed to the oxidative stress induced by the generated ROS,[49,50] and the antibacterial action mechanism is the same as for Ag NPs. However, the cytotoxicity of Ag NPs is lower than that of Ag^+, and the toxicity of Ag NPs is closely related to the structure, crystal defects, *etc.*[51] ROS induction is a vital cause of the cytotoxicity of Ag NPs, and it also is the key product that can interfere with or inhibit the growth of bacteria. In this work, the composite fillers MA or MAC were slightly embedded into the coating system, and the coating network acted as the reservoir to release Ag^+ from the Ag NPs on the solid surface. It could be speculated that there were few Ag^+ enriched on the coating surface when the target composite coating was utilized as a protection for the solid surface, but the composite coating still developed an excellent antibacterial property, as shown in the above-mentioned results and as shown in Fig. 6.

4. Conclusion

In summary, we fabricated a simple and effective strategy to construct stable a 3D $Ti_3C_2T_x$ MXene@cellulose@Ag (MAC) composite *via* the process of a direct grafting, precise capture, integration with anchors, and tailored loading for boosting the storage of Ag NPs on the MXene surface. Owing to the synergistic effect of the modified MXene as a carrier and Ag as the target load to achieve the expected functions, the MAC composite filler could serve as a potential antibacterial material in the antifouling coating field thanks to its higher loading capability, better stability, and high antibacterial performance. These properties could promote the compatibility between MAC and the coating network, and avoid Ag NPs aggregation in the coating system. This work proposes a simple method for the fabrication of a MXene composite filler, and gives a deep insight into different dimensional nanofillers to be assessed to develop synergistic effects for adjusting the antibacterial attachment property of polybenzoxazine coating.

Conflicts of interest

There are no conflicts to declare.

Acknowledgements

The authors thank for Fujian Province Natural Science Foundation project (grant no. 2023J05157), Fujian Young and Middle-Aged Teacher Education Research Project (grant no. JAT220184), Scientific Research School Foundation (grant no. C622150).

References

1 F. Dixit, K. Zimmermann, R. Dutta, N. J. Prakash, B. Barbeau, M. Mohseni and B. Kandasubramanian, Application of MXenes for water treatment and energy-efficient desalination: A review, *J. Hazard. Mater.*, 2021, **423**, 127050, DOI: 10.1016/j.jhazmat.2021.127050.

2 Y. Wu, X. Li, H. Zhao, F. Yao, J. Cao, Z. Chen, X. Huang, D. Wang and Q. Yang, Recent advances in transition metal carbides and nitrides (MXenes): Characteristics, environmental remediation and challenges, *Chem. Eng. J.*, 2021, **418**, 129296, DOI: 10.1016/j.cej.2021.129296.

3 M. Naguib, M. Kurtoglu, V. Presser, J. Lu, J. Niu, M. Heon, L. Hultman, Y. Gogotsi and M. W. Barsoum, Two-Dimensional Nanocrystals Produced by Exfoliation of Ti_3AlC_2, *Adv. Mater.*, 2011, **23**(37), 4248–4253, DOI: 10.1002/adma.201102306.

4 Q. Shen, C. Chen, J. Long and S. Wang, Reproducible 2D $Ti_3C_2T_x$ for perovskite-based photovoltaic device, *RSC Adv.*, 2023, **13**, 9555–9562, DOI: 10.1039/d2ra08088e.

5 D. Zhao, R. Zhao, S. Dong, X. Miao, Z. Zhang, C. Wang and L. Yin, Alkali-induced 3D crinkled porous Ti_3C_2 MXene architectures coupled with NiCoP bimetallic phosphide nanoparticles as anodes for high-performance sodium-ion batteries, *Energy Environ. Sci.*, 2019, **12**(8), 2422–2432, DOI: 10.1039/c9ee00308h.

6 A. Vaughn, J. Ball, T. Heil, D. J. Morgan, G. I. Lampronti, G. Maršalkaitė, C. L. Raston, N. P. Power and S. Kellici, Selective Calixarene-Directed Synthesis of MXene Plates, Crumpled Sheets, Spheres, and Scrolls, *Chem.–Eur. J.*, 2017, **23**(34), 8128–8133, DOI: 10.1002/chem.201701702.

7 L. Wang, X. Yao, S. Yuan, Y. Gao, R. Zhang, X. Yu, S.-T. Tu and S. Chen, Ultra-high performance humidity sensor enabled by a self-assembled $CuO/Ti_3C_2T_X$ MXene, *RSC Adv.*, 2023, **13**(9), 6264–6273, DOI: 10.1039/d2ra06903b.

8 M. W. Barsoum and M. Radovic, Elastic and Mechanical Properties of the MAX Phases, *Annu. Rev. Mater. Sci.*, 2011, **41**, 195–227, DOI: 10.1146/annurev-matsci-062910-100448.

9 W. Hu, Z. Huang, Y. Wang, X. Li, H. Zhai, Y. Zhou and L. Chen, Layered ternary MAX phases and their MX particulate derivative reinforced metal matrix composite:A review, *J. Alloys Compd.*, 2021, **856**, 157313, DOI: 10.1016/j.jallcom.2020.157313.

10 C. J. Zhang, S. Pinilla, N. McEvoy, C. P. Cullen, B. Anasori, E. Long, S.-H. Park, A. Seral-Ascaso, A. Shmeliov, D. Krishnan, C. Morant, X. Liu, G. S. Duesberg, Y. Gogotsi and V. Nicolosi, Oxidation Stability of Colloidal Two-Dimensional Titanium Carbides (MXenes), *Chem. Mater.*, 2017, **29**(11), 4848–4856, DOI: 10.1021/acs.chemmater.7b00745.

11 X. Qin, Z. Wu, J. Fang, S. Li, S. Tang and X. Wang, MXene-intercalated montmorillonite nanocomposites for long-acting antibacterial, *Appl. Surf. Sci.*, 2023, **616**, 156521, DOI: 10.1016/j.apsusc.2023.156521.

12 D. Mengna, S. Xinyu, B. Tong, Z. Hui, W. Jiao, H. Kunyi, L. Lihua, L. Zhenyu and W. Li, MXene-intercalated montmorillonite nanocomposites for long-acting antibacterial, *Composites, Part B*, 2021, **230**, 109498, DOI: 10.1016/j.compositesb.2021.109498.

13 D. Haibin, Z. Shaohua, Y. Liguo, W. Na, C. Shaojuan, M. Jianwei and L. Jiwei, Cu/Zn galvanic couples composite antibacterial dressings prepared by template-assisted magnetron sputtering, *Composites, Part B*, 2021, **224**, 109240, DOI: 10.1016/j.compositesb.2021.109240.

14 J. L. Falconer, J. A. Alt and D. W. Grainger, Comparing *ex vivo* and *in vitro* translocation of silver nanoparticles and ions through human nasal epithelium, *Biomaterials*, 2018, **171**, 97–106, DOI: 10.1016/j.biomaterials.2018.04.013.

15 P. R. Cáceres-Vélez, M. L. Fascineli, M. H. Sousa, C. K. Grisolia, L. Yate, P. E. N. de Souza, I. Estrela-Lopis, S. Moya and R. B. Azevedo, Humic acid attenuation of silver nanoparticle toxicity by ion complexation and the formation of a Ag^{3+} coating, *J. Hazard. Mater.*, 2018, **353**, 173–181, DOI: 10.1016/j.jhazmat.2018.04.019.

16 S. Parham, M. Nemati, S. Sadir, S. Bagherbaigi, D. H. B. Wicaksono and H. Nur, *In Situ* Synthesis of Silver Nanoparticles for Ag-NP/Cotton Nanocomposite and Its Bactericidal Effect, *J. Chin. Chem. Soc.*, 2017, **64**(11), 1286–1293, DOI: 10.1002/jccs.201700157.

17 Q. Feng, J. Wu, G. Chen, F. Cui, T. Kim and J. Kim, A mechanistic study of the antibacterial effect of silver ions on *Escherichia coli* and *Staphylococcus aureus*, *J. Biomed. Mater. Res.*, 2000, **52**(4), 662–668, DOI: 10.1002/1097-4636(20001215)52:4<662::aid-jbm10>3.0.co;2-3.

18 H. Wang, M. Wang, X. Xu, P. Gao, Z. Xu, Q. Zhang, H. Li, A. Yan, R. Y.-T. Kao and H. Sun, Multi-target mode of action of silver against *Staphylococcus aureus* endows it with capability to combat antibiotic resistance, *Nat. Commun.*, 2021, **12**, 3331, DOI: 10.1038/s41467-021-23659-y.

19 J. Hu, J. Lin, Y. Zhang, Z. Lin, Z. Qiao, Z. Liu, W. Yang, X. Liu, M. Dong and Z. Guo, A new anti-biofilm strategy of enabling arbitrary surfaces of materials and devices with robust bacterial anti-adhesion *via* a spraying modified microsphere method, *J. Mater. Chem. A*, 2019, **7**(45), 26039–26052, DOI: 10.1039/c9ta07236e.

20 C. Shuai, G. Liu, Y. Yang, F. Qi, S. Peng, W. Yang, C. He, G. Wang and G. Qian, A strawberry-like Ag-decorated barium titanate enhances piezoelectric and antibacterial activities of polymer scaffold, *Nano Energy*, 2020, **74**, 104825, DOI: 10.1016/j.nanoen.2020.104825.

21 S. Luo, L. Fan, K. Yang, Z. Zhong, X. Wu and T. Ren, *In situ* and controllable synthesis of Ag NPs in tannic acid-based hyperbranched waterborne polyurethanes to prepare antibacterial polyurethanes/Ag NPs composites, *RSC Adv.*, 2018, **8**(64), 36571–36578, DOI: 10.1039/c8ra07575a.

22 J. Peng, H. Pengfei, L. Xu and L. Kun, Titanium carbide MXenes-initiated plasmonic metal-support interaction for effective photocatalysis on uncoated Ag nanoparticles, *Appl. Surf. Sci.*, 2022, **612**, 155850, DOI: 10.1016/j.apsusc.2022.155850.

23 Y. Zhou, M. Liu, Y. Wang, J. Yuan and X. Men, Significance of constructed MXene@Ag hybrids for enhancing the mechanical and tribological performance of epoxy composites, *Tribol. Int.*, 2021, **165**, 107328, DOI: 10.1016/j.triboint.2021.107328.

24 Y. Deng, L. Xia, G.-L. Song, Y. Zhao, Y. Zhang, Y. Xu and D. Zheng, Development of a curcumin-based antifouling and anticorrosion sustainable polybenzoxazine resin composite coating, *Composites, Part B*, 2021, **225**, 109263, DOI: 10.1016/j.compositesb.2021.109263.

25 Y. Deng, G.-L. Song, T. Zhang, Z. Lang, P. Wu and D. Zheng, Loading halloysite nanotubes on MXene as functional composite filler towards a polybenzoxazine anticorrosion coating, *Colloids Surf., A*, 2022, **650**, 129498, DOI: 10.1016/j.colsurfa.2022.129498.

26 Y. Sun and Y. Xia, Mechanistic Study on the Replacement Reaction between Silver Nanostructures and Chloroauric Acid in Aqueous Medium, *J. Am. Chem. Soc.*, 2004, **126**(12), 3892–3901, DOI: 10.1021/ja039734c.

27 Y. Deng, G.-L. Song, T. Zhang, L. Xia, Y. Zhao and D. Zheng, The controlled *in-situ* growth of silver-halloysite

nanostructure *via* interaction bonds to reinforce a novel polybenzoxazine composite resin and improve its antifouling and anticorrosion properties, *Compos. Sci. Technol.*, 2022, **221**, 109312, DOI: 10.1016/j.compscitech.2022.109312.

28 Y. Deng, G.-L. Song, D. Zheng and Y. Zhang, Fabrication and synergistic antibacterial and antifouling effect of an organic/inorganic hybrid coating embedded with nanocomposite Ag@TA-SiO_2 particles, *Colloids Surf., A*, 2020, **613**, 126085, DOI: 10.1016/j.colsurfa.2020.126085.

29 C. Liang, Y. Meng, Y. Zhang, H. Zhang, W. Wang, M. Lu and G. Wang, Insights into the impact of interlayer spacing on MXene-based electrodes for supercapacitors: A review, *J. Energy Storage*, 2023, **65**, 107341, DOI: 10.1016/j.est.2023.107341.

30 Y. Luo, Y. Tian, Y. Tang, X. Yin and W. Que, 2D hierarchical nickel cobalt sulfides coupled with ultrathin titanium carbide (MXene) nanosheets for hybrid supercapacitors, *J. Power Sources*, 2020, **482**, 228961, DOI: 10.1016/j.jpowsour.2020.228961.

31 O. Mashtalir, M. Naguib, V. N. Mochalin, Y. Dall'Agnese, M. Heon, M. W. Barsoum and Y. Gogotsi, Intercalation and delamination of layered carbides and carbonitrides, *Nat. Commun.*, 2013, **4**, 1716, DOI: 10.1038/ncomms2664.

32 Z. Lang, Z. Zhuang, S. Li, L. Xia, Y. Zhao, Y. Zhao, C. Han and L. Zhou, MXene Surface Terminations Enable Strong Metal-Support Interactions for Efficient Methanol Oxidation on Palladium, *ACS Appl. Mater. Interfaces*, 2020, **12**(2), 2400–2406, DOI: 10.1021/acsami.9b17088.

33 Q. Feng, Y. Zhan, W. Yang, H. Dong, A. Su, L. Li, X. Chen and Y. Chen, Ultra-high flux and synergistically enhanced anti-fouling Ag@MXene lamellar membrane for the fast purification of oily wastewater through nano-intercalation, photocatalytic self-cleaning and antibacterial effect, *Sep. Purif. Technol.*, 2022, **298**, 121635, DOI: 10.1016/j.seppur.2022.121635.

34 J. Jin, T. Iyoda, C. Cao, Y. Song, L. Jiang, T. J. Li and D. B. Zhu, Self-Assembly of Uniform Spherical Aggregates of Magnetic Nanoparticles through π-π Interactions, *Angew. Chem., Int. Ed.*, 2001, **40**(11), 2135–2138, DOI: 10.1002/1521-3773(20010601)40:11<2135::aid-anie2135>3.0.co;2-o.

35 Z. Wang, C. Duan, Y. Zhou, F. Wang, Q. Lu, D. Liu, F. Wang and X. Meng, Ag Decorated 3D Honeycomb-like MXene Architecture as an Advanced Lithium-ion Anode Material towards High Capacity and Long-term Cycle Capability, *Appl. Surf. Sci.*, 2023, **615**, 156406, DOI: 10.1016/j.apsusc.2023.156406.

36 D. Rawtani, G. Pandey, M. Tharmavaram, P. Pathak, S. Akkireddy and Y. K. Agrawal, Development of a novel 'nanocarrier' system based on Halloysite Nanotubes to overcome the complexation of ciprofloxacin with iron: An *in vitro* approach, *Appl. Clay Sci.*, 2017, **150**(15), 293–302, DOI: 10.1016/j.clay.2017.10.002.

37 K. Jlassi, S. Mallick, H. Mutahir, Z. Ahmad and F. Touati, Synthesis of *In Situ* Photoinduced Halloysite-Polypyrrole@Silver Nanocomposite for the Potential Application in Humidity Sensors, *Nanomaterials*, 2020, **10**(7), 1426, DOI: 10.3390/nano10071426.

38 G. Yang, F. Liu, J. Zhao, L. Fu, Y. Gu, L. Qu, C. Zhu, J.-J. Zhu and Y. Lin, MXenes-based nanomaterials for biosensing and biomedicine, *Coord. Chem. Rev.*, 2023, **479**, 215002, DOI: 10.1016/j.ccr.2022.215002.

39 S. M. George and B. Kandasubramanian, Advancements in MXene-Polymer composites for various biomedical applications, *Ceram. Int.*, 2020, **46**(7), 8522–8535, DOI: 10.1016/j.ceramint.2019.12.257.

40 F. Seidi, A. Arabi Shamsabadi, M. Dadashi Firouzjaei, M. Elliott, M. R. Saeb, Y. Huang, C. Li, H. Xiao and B. Anasori, MXenes Antibacterial Properties and Applications: A Review and Perspective, *Small*, 2023, **19**(14), 2206716, DOI: 10.1002/smll.202206716.

41 F. Fu, L. Li, L. Liu, J. Cai, Y. Zhang, J. Zhou and L. Zhang, Construction of Cellulose Based ZnO Nanocomposite Films with Antibacterial Properties through One-Step Coagulation, *ACS Appl. Mater. Interfaces*, 2015, **7**(4), 2597–2606, DOI: 10.1021/am507639b.

42 W. Hu, C. Peng, W. Luo, M. Lv, X. Li, D. Li, Q. Huang and C. Fan, Graphene-Based Antibacterial Paper, *ACS Nano*, 2010, **4**(7), 4317–4323, DOI: 10.1021/nn101097v.

43 Y.-X. Hou, H. Abdullah, D.-H. Kuo, S.-J. Leu, N. S. Gultom and C.-H. Su, A comparison study of SiO_2/nano metal oxide composite sphere for antibacterial application, *Composites, Part B*, 2018, **133**(15), 166–176, DOI: 10.1016/j.compositesb.2017.09.021.

44 S. P. Deshmukh, S. M. Patil, S. B. Mullani and S. D. Delekar, Silver nanoparticles as an effective disinfectant: A review, *Biomater. Adv.*, 2019, **97**, 954–956, DOI: 10.1016/j.msec.2018.12.102.

45 C. Tong, W. Zou, W. Ning, J. Fan, L. Li, B. Liu and X. Liu, Synthesis of DNA-guided silver nanoparticles on a graphene oxide surface: enhancing the antibacterial effect and the wound healing activity, *RSC Adv.*, 2018, **8**(49), 28238–28248, DOI: 10.1039/c8ra04933e.

46 B. González-Flecha and B. Demple, Metabolic Sources of Hydrogen Peroxide in Aerobically Growing *Escherichia coli*, *J. Biol. Chem.*, 1995, **270**(23), 13681–13687, DOI: 10.1074/jbc.270.23.13681.

47 C. Carlson, S. M. Hussain, A. M. Schrand, L. K. Braydich-Stolle, K. L. Hess, R. L. Jones and J. J. Schlager, Unique Cellular Interaction of Silver Nanoparticles: Size-Dependent Generation of Reactive Oxygen Species, *J. Phys. Chem. B*, 2008, **112**(43), 13608–13619, DOI: 10.1021/jp712087m.

48 H. Su, C. Chou, D. Hung, S. Lin, I. Pao, J. Lin, F. Huang, R. Dong and J. Lin, The disruption of bacterial membrane integrity through ROS generation induced by nanohybrids of silver and clay, *Biomaterials*, 2009, **30**(30), 5979–5987, DOI: 10.1016/j.biomaterials.2009.07.030.

49 G. P. Lim, C. F. Soon, N. L. Ma, M. Morsin, N. Nayan, M. K. Ahmad and K. S. Tee, Cytotoxicity of MXene-based nanomaterials for biomedical applications: A mini review, *Environ. Res.*, 2021, **201**, 111592, DOI: 10.1016/j.envres.2021.111592.

50 G. A. Naikoo, F. Arshad, M. Almas, I. U. Hassan, M. Z. Pedram, A. A. A. Aljabali, V. Mishra, Á. Serrano-Aroca, M. Birkett, N. B. Charbe, R. Goyal, P. Negi, M. El-Tanani and M. M. Tambuwala, 2D materials, synthesis, characterization and toxicity: A critical review, *Chem.–Biol. Interact.*, 2022, **365**(25), 110081, DOI: **10.1016/j.cbi.2022.110081**.

51 S. George, S. Lin, Z. Ji, C. R. Thomas, L. Li, M. Mecklenburg, H. Meng, X. Wang, H. Zhang, T. Xia, J. N. Hohman, S. Lin, J. I. Zink, P. S. Weiss and A. E. Nel, Surface Defects on Plate-Shaped Silver Nanoparticles Contribute to Its Hazard Potential in a Fish Gill Cell Line and Zebrafish Embryos, *ACS Nano*, 2012, **6**(5), 3745–3759, DOI: **10.1021/nn204671v**.